



## Article

# Finite Element and Machine Learning-Based Prediction of Buckling Strength in Additively Manufactured Lattice Stiffened Panels

Saiaf Bin Rayhan <sup>1,\*</sup>, Md Mazedur Rahman <sup>2</sup>, Jakiya Sultana <sup>2</sup>, Szabolcs Szávai <sup>2</sup> and Gyula Varga <sup>2,\*</sup>

<sup>1</sup> Department of Aeronautical Engineering, Bangabandhu Sheikh Mujibur Rahman Aviation and Aerospace University, Lalmonirhat 5500, Bangladesh

<sup>2</sup> Faculty of Mechanical Engineering and Informatics, University of Miskolc, H-3515 Miskolc, Hungary; md.mazedur.rahman@student.uni-miskolc.hu (M.M.R.); jakiya.sultana@student.uni-miskolc.hu (J.S.); szabolcs.szavai@uni-miskolc.hu (S.S.)

\* Correspondence: rayhan.saiaf@mail.nwpu.edu.cn (S.B.R.); gyula.varga@uni-miskolc.hu (G.V.)

**Abstract:** The current research aimed to investigate the critical buckling load of a simply supported aerospace-grade stiffened panel made of additively manufactured cubic lattice unit cell arrays, namely simple cubic, face-centered cubic (FCC) and body-centered cubic (BCC) structures. Ansys Design Modeler was chosen to design and analyze the critical buckling load of the panel, while a popular material, Ti-6Al-4V, was used as the build material. Numerical validation on both the stiffened panel and a lattice beam structure was established from multiple resources from the literature. Finally, the panels were tested against increments of a strut diameter ranging from 0.5 mm to 2 mm, which corresponds to a relative density of 6% to 78%. It was found that considering the relative density and fixed relative density, the simple cubic lattice cell outperformed the buckling results of the FCC and BCC panels. Moreover, the relationship of the parameters was found to be non-linear. Finally, the data samples collected from numerical outcomes were utilized to train four different machine learning models, namely multi-variable linear regression, polynomial regression, the random forest regressor and the K-nearest neighbor regressor. The evaluation metrics suggest that polynomial regression provides the highest accuracy among all the tested models, with the lowest mean squared error (MSE) value of 0.0001 and a perfect  $R^2$  score. The current research opens up the discussion of using cubic lattice cells as potential structures for future stiffened panels.



Academic Editor: Umberto Prisco

Received: 17 December 2024

Revised: 6 January 2025

Accepted: 9 January 2025

Published: 17 January 2025

**Citation:** Rayhan, S.B.; Rahman, M.M.; Sultana, J.; Szávai, S.; Varga, G. Finite Element and Machine Learning-Based Prediction of Buckling Strength in Additively Manufactured Lattice Stiffened Panels. *Metals* **2025**, *15*, 81. <https://doi.org/10.3390/met15010081>

**Copyright:** © 2025 by the authors. Licensee MDPI, Basel, Switzerland. This article is an open access article distributed under the terms and conditions of the Creative Commons Attribution (CC BY) license (<https://creativecommons.org/licenses/by/4.0/>).

**Keywords:** ML algorithms; FEA; lattice unit cell; critical buckling load; additive manufacturing

## 1. Introduction

Lattice structures are created by intentional voids to reduce the structure's weight, which mainly benefits from decreasing manufacturing costs and reducing waste without compromising the mechanical properties and performance compared to traditional blocks [1]. Particularly in aerospace industries, they are employed to enhance fuel efficiency, which is more than 6–8%, by reducing the weight of the overall structure by 8–10% compared to conventional structures or materials [2].

A wide variety of materials and manufacturing methods are used to design and fabricate lattice structures. However, focusing on the aerospace industry, metal materials are the primary choice, as they exhibit excellent mechanical properties, including superior strength and corrosion resistance, and can perform better in different weather and harsh environments than polymers or other materials [3]. On the other hand, a metal-based lattice structure can offer more desirable performance, such as better heat transfer and

insulation, noise insulation and shock absorption, compared to conventional metallic foams or honeycomb structures [3,4]. Furthermore, it can outperform the honeycomb in terms of energy absorption [5]. An earlier study compared the impact behavior of lattice and honeycomb structures and found that lattice structures offered better impact resistance than honeycomb structures [6]. Selective laser melting (SLM), a well-known additive manufacturing technique, is used to fabricate lattice-structure-based metal components. While post-processing is often required to improve a surface finish, SLM offers superior mechanical properties, including strength and is more efficient in controlling the waste of raw materials compared to other manufacturing methods [7,8].

Compressive behavior testing is the most commonly employed and convenient testing method for understanding the mechanical behavior of SLM-fabricated metallic lattice structures. For example, the compressive behavior of a newly developed circular cell-based metal lattice structure is tested experimentally and compared with a BCC cell structure [9]. The investigation found that a circular cell-based lattice provided excellent compressive strength and stiffness compared to a BCC structure of a higher density. A similar experimental study was conducted based on trabecular and triply periodic minimal-surface-based lattice structures made of Ti-6Al-4V via SLM. The investigation revealed that the trabecular lattice showed a compressive modulus of 5.58 GPa, while the triply periodic minimal-surface-based lattice provided a compressive modulus of 5.51 GPa. These satisfactory moduli can help mitigate the stress-shielding effect, particularly in bone joint applications [10]. Similarly, a hybrid lattice structure fabricated from 316 L stainless steel was printed by SLM and investigated for compressive behavior, which is a combination of an octet cell and a rhombic dodecahedron (RD) cell. The outcomes revealed that this proposed lattice demonstrated improved energy absorption capabilities ( $1.203 \text{ MJ/m}^3$ ), which may help improve resistance to process-induced geometric imperfections [11]. To compute the mechanical properties of a lattice, the finite element method (FEM) is widely adopted as a cost-effective tool to compute the mechanical properties of metallic lattice structures. It provides responses comparable to experimental outcomes, while providing cost-effective solutions. Thus, a significant number of studies have been employed based on computational analysis to estimate the mechanical performance of metallic structures, including the impact of defects and local irregularities, with agreeable deviation from the experiments [12–15]. In lattice structures, different types of cells, strut diameters, unit cell types, repeating units, relative densities, and material types can remarkably influence mechanical properties [9,11,16–18]. For instance, a monotonical relationship between the strut diameter and load-bearing capacity has been observed in aluminum-based cellular lattice structures [17]. Similarly, with an increase in relative density, a lattice can experience a similar failure pattern as its solid counterpart [16].

Buckling is one of the primary failure criteria of an aircraft structure, and panels stiffened with different stiffeners are widely used to resist buckling [12]. A number of buckling and post-buckling studies have been carried out on isotropic- and composite-based stiffened panels under compressing loading based on analytical, numerical and experimental solutions [13,14]. A study suggests that a closed-hat stiffened panel is better at resisting buckling and post-buckling failure than open-hat and Z-type stiffened panels [15]. Moreover, the bio-inspired Voronoi stiffener can significantly reduce the weight while improving the buckling strength of a stiffened panel when compared to conventional ones such as isogrid, orthogrid and stringer structures [19]. Another study on the straight and inclined positions of stiffeners on a stiffened panel revealed that the inclined one had a greater post-buckling load-carrying capacity, meaning it has the potential to be used in aircraft panels [20]. An innovative design adopting a closely positioned Y-shaped stiffener geometry with transverse stiffeners suggests that the configuration can significantly improve

the buckling and ultimate collapse loading of the aircraft panel [21]. To understand the buckling and post-buckling failure of additively manufactured lattice columns, an experimental and numerical investigation was carried out, and it was revealed that in a column with same the mass, dimensions and relative density, a larger unit cell size exhibited higher buckling resistance [22]. A similar study on the porosity of a beam concluded that critical buckling load was improved in the case of increasing the volume fraction near the middle surface or the two edges of the beam [23].

In recent times, machine learning algorithms have been extensively used to predict the buckling of structures, as they can significantly reduce the time of prediction with excellent accuracy once trained. A study based on the various cross-sectional geometries of thin-walled channels consisting of 4608 samples was trained using an Artificial Neural Network (ANN) algorithm and found that the model accurately predicted 98% of data [24]. Another study compared three different hybrid machine learning approaches to predict the critical buckling load of an I-beam with circular cutouts. They found that the ANFIS-SFLA hybrid algorithm was the best at predicting the critical buckling load with the highest accuracy, achieving a mean absolute error (MAE) of 0.017 [25]. A similar study on a composite shell buckling with 11,000 cases suggested that deep learning models can significantly improve prediction accuracy compared to classical models such as random forest regressor, decision tree regressor and multivariable linear regression [26]. Several ML algorithms such as decision tree, random forest, K-nearest neighbor (KNN), extreme gradient boosting (XGBoost), etc., were used to predict the buckling of steel columns with hyperparameter tuning, and it was found that all of the models predicted the behavior with similar accuracy [27]. Ten different ML algorithms were used to predict the nominal buckling stress of steel shear panel dampers, and it was revealed that the ANN model provided the highest accuracy, with a root mean squared error (RMSE) of 0.0094 [28]. A similar conclusion was also made upon comparing the best ML models for the buckling prediction of a bi-directional FG micro beam [29]. Next, the critical buckling load of a carbon-nanotube (CNT)-reinforced hybrid functionally graded plate was studied using FEM, and the data were utilized to train deep neural network, XGBoost and random forest ML models. The study concluded that the deep neural network outperformed XGBoost and random forest models in terms of buckling load prediction [30]. A very recent study on predicting the buckling load of a composite cylinder suggested that random forest and XGBoost were the best models for predicting buckling pressure, while ANN and support vector regression (SVR) showed reasonable accuracy [31]. Another recent study on the prediction of the buckling strength of thin-walled composite structures suggested that both random forest and gradient boosting could be implemented successfully under mechanical and thermal loading conditions [30].

Lattice cubic cells present a promising opportunity for lightweight structural design, particularly in the aerospace industry. While previous studies have extensively analyzed the mechanical behavior of these cells, critical gaps remain, specifically in calculating the critical buckling load and evaluating their performance as realistic structural components. Secondly, buckling, as a primary failure criterion, has been widely studied in stiffened panels, with the literature exploring various innovative designs. However, the potential of utilizing lattice cubic cells as foundational building blocks for stiffened panels remains unexplored.

This study addresses these gaps by proposing lattice cubic cells as a viable building block for stiffened panels and integrating machine learning (ML) algorithms to predict the critical buckling load. The current research is outlined as follows: Section 2 describes the computational modeling and setup of the current study. Section 3 provides an overview of the machine learning (ML) algorithms employed in this research to predict the critical

buckling load, along with the detailed ML workflow. Section 4 validates the numerical analysis methods used to evaluate the critical buckling load for both the stiffened panel and the lattice column. Section 5 presents a critical analysis of the parameters influencing the buckling behavior of the lattice stiffened panel and compares the performance of various ML models to determine their accuracy in predicting the critical buckling load. Finally, Section 6 summarizes the key findings of the research and outlines the potential future directions for this study.

## 2. Computational Modeling and Setup

For the present study, a stiffened panel with a length of 490 mm and a width of 275 mm was designed with 6566 repeated lattice unit cells. The thickness of the panel was 5 mm, corresponding to the height of a single unit cell. The height of the stiffener was 25 mm, consisting of 5-unit cells. The height, length and width of the unit cells were 5 mm each, while the design of the unit cells was simple cubic, face-centered cubic (FCC) and body-centered cubic (BCC). Finally, the diameter of the strut was considered to be 0.5 mm to 2 mm in order to compare the buckling performance of the panels consisting of three different types of cubic lattice cells specified earlier. Schematic representations of the stiffened panel and the single-unit cells are illustrated in Figure 1.

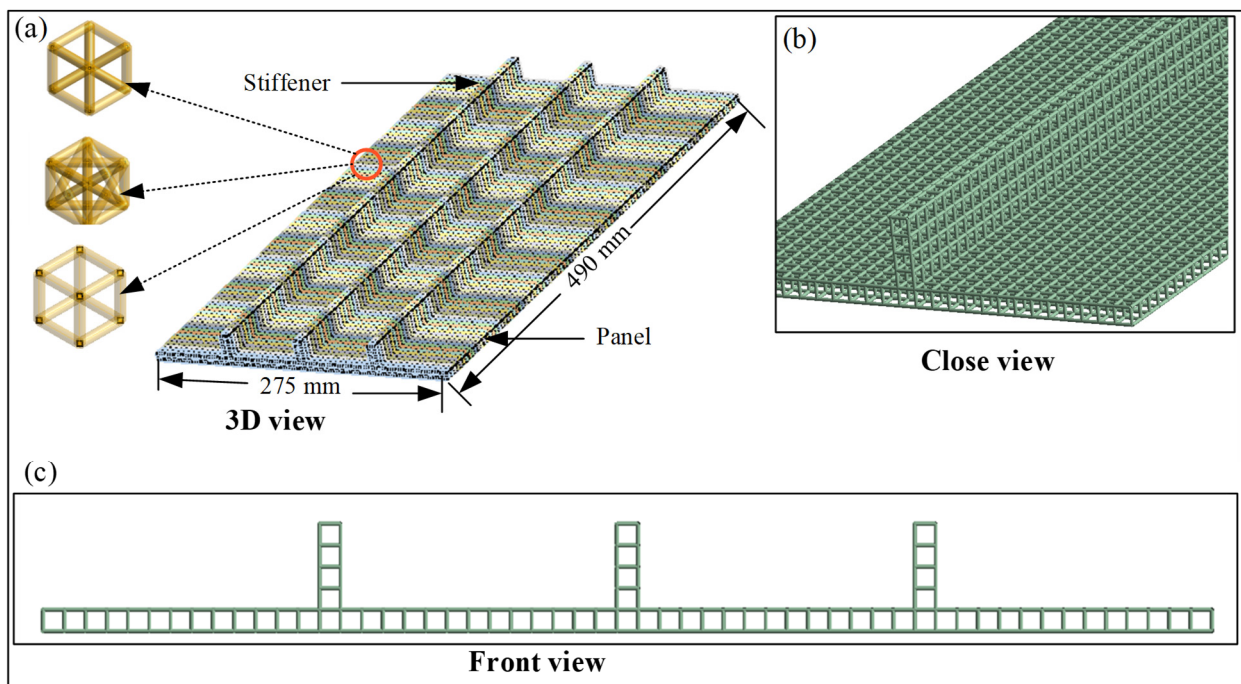


**Figure 1.** (a) Three-dimensional model of stiffener panel with different lattice structures, (b) close view of lattice stiffener panel and (c) front view of designed stiffener panel.

Next, for the material selection, titanium alloy Ti-6Al-4V, a popular choice for additively manufactured lattice cells, was employed. The mechanical properties required for elastic buckling, namely a Young's modulus  $E = 112$  GPa and Poisson's ratio  $\mu = 0.35$ , were chosen from the available literature, along with a density  $\rho = 4420$  Kg/m<sup>3</sup>, for the calculation of the relative density and porosity of the lattice structure [32].

For the numerical analysis, line bodies were selected to design the lattice-stiffened panels, which create beam elements after mesh generation. This can significantly reduce the cost of computational time and provide good accuracy [22]. In the validation section, lattice columns are also made of beam elements, which exhibit a good correlation with the numerical data. The element size was kept at 2.5 mm, as further reducing this size would

cause an increase in computation time without significantly improving the outcomes. The meshed body of the lattice cell is shown in Figure 2. Finally, for the boundary condition, a fixed–fixed boundary condition was chosen for the shorter edges of the stiffened panel, while the longer edges were kept free to compute the critical buckling load, similar to the conditions found for aircraft stiffened panels in the literature [33].

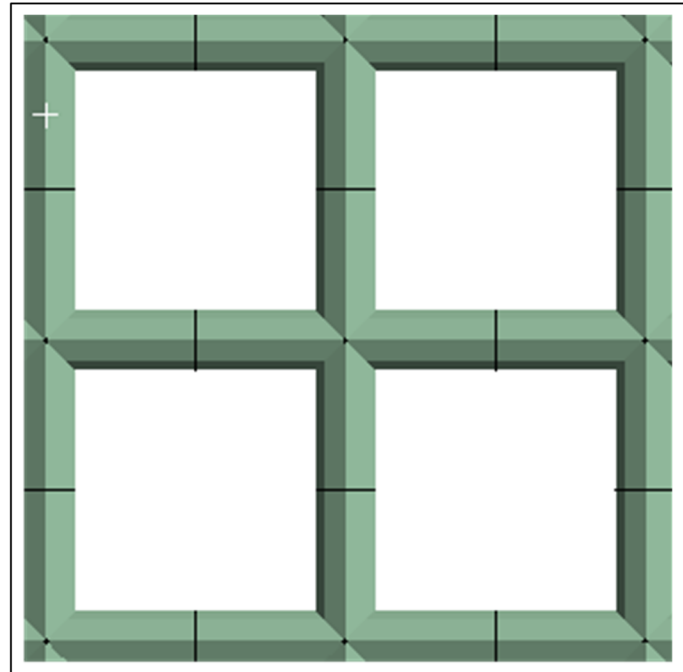


**Figure 2.** Generated meshed body of the lattice cell.

### 3. Machine Learning Models

#### 3.1. Multivariable Linear Regression

Multivariable linear regression is one of the most fundamental machine learning models, which creates a linear hyperplane in n-dimensional space with respect to its variables, also called features and coefficients. In contrast to simple linear regression, which is defined by  $y=b_0+b_1x$ , where  $y$  is the target variable and  $x$  is the single independent variable, multivariable linear regression may have n number of independent variables, such as  $x_1, x_2, x_3, \dots, x_n$ , and the equation becomes [34]

$$y=b_0+b_1x_1+b_2x_2+b_3x_3+\dots+b_nx_n \quad (1)$$

where  $b_1, b_2, b_3, \dots, b_n$  are the coefficients, and  $b_0$  is the intercept when the other terms are zero.

In the multivariable linear regression, the hyperplane is adjusted iteratively by minimizing the mean squared error (MSE), which is defined as [35]:

$$MSE=\frac{1}{m}\sum_{i=1}^m (y_i-\hat{y}_i)^2 \quad (2)$$

where  $y_i$ = actual value of the i-th data,  $\hat{y}_i$ = predicted value of the i-th data and m is the number of data points. In machine learning, MSE is used as the cost function, and an iterative optimization algorithm called gradient descent is applied to minimize the cost function by finding the optimal coefficients  $b_0, b_1, b_2, b_3, \dots, b_n$ . The algorithm computes the gradients

of the cost function with respect to each coefficient and updates them iteratively to reduce the error. For a simple linear regression, Equation (2) can be expressed as:

$$MSE = \frac{1}{n} \sum_{i=1}^n (y_i - (bx_1 + b_0))^2 \quad (3)$$

And the gradients can be found as

$$\frac{\partial}{\partial b} = \frac{2}{n} \sum_{i=1}^n -x_i (y_i - (bx_1 + b_0)) \quad (4)$$

$$\frac{\partial}{\partial b_0} = \frac{2}{n} \sum_{i=1}^n -(y_i - (bx_1 + b_0)) \quad (5)$$

Initially, a random value is selected to calculate the coefficients,  $b$  and  $b_0$ , and after that, new values are calculated as:

$$b = b - \text{learning rate} \times \frac{\partial}{\partial b} \quad (6)$$

$$b_0 = b_0 - \text{learning rate} \times \frac{\partial}{\partial b_0} \quad (7)$$

where the learning rate determines the step size at each iteration while progressing towards the minimum MSE. An example of using gradient descent to optimize the cost function is shown in Figure 3a,b [36,37].

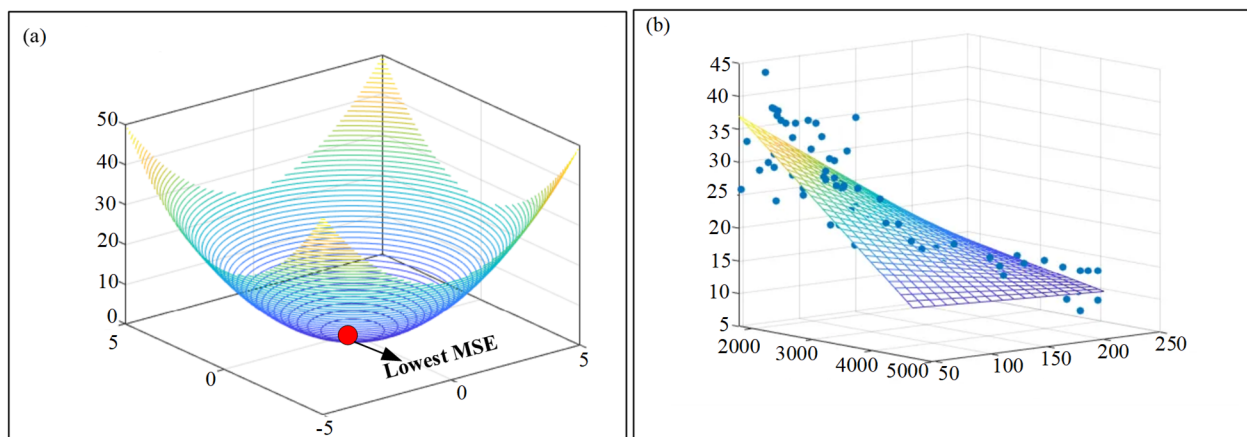


Figure 3. (a) Lowest MSE point and (b) gradient descent to optimize the cost function.

### 3.2. Polynomial Regression

Unlike multivariable linear regression, which predicts a linear hyperplane between the independent variables and the target variable, polynomial regression is an extension to  $n$ -degree polynomials that is capable of capturing non-linear relationships among the features. The mathematical expression can be defined as [38]:

$$y = b_0 + b_1x + b_2x^2 + b_3x^3 + \dots + b_nx^n \quad (8)$$

where  $x$  is the independent variable and  $x^2, x^3, \dots, x^n$  are the higher-order terms of the independent variable.  $b_0, b_1, b_2, \dots, b_n$  are the coefficients of the polynomials. In the case of multivariable independent variables, the polynomial expression involves cross-products and higher-order terms like  $x_1^2, x_1x_2, x_2^3$ , etc.

The calculation of MSE and gradient descent is the same as in multivariable linear regression except they include the higher-order terms as well.

### 3.3. KNN (K-Nearest Neighbor) Regressor

KNN is a widely used supervised machine learning algorithm for its simplicity and ease of implementation in both classification and regression problems. The working principal of KNN is based on finding neighbors of similar data points that have already been trained. Neighbors among the trained datasets are chosen using a distance metric, such as Euclidean distance, given as [39]:

$$d(x_{test}, x_{train}) = \sqrt{\sum_{i=1}^n (x_{test,i} - x_{train,i})^2} \quad (9)$$

The value of K, which defines the number of neighbors for the new data point, has a significant impact on the prediction of new data. This requires a parametric study, such as the GridSearchCV algorithm, to find the optimal value of K for the best-fitted predictions with the lowest MSE. For instance, if K is chosen as 2, the new data point will be placed such that it has two neighbors with the least distance calculated from Equation (9) among the trained data points, and the average of the two neighbors is calculated to predict the value of the new data. An illustration, Figure 4a, is drawn to show the neighbors of new data points A and B. The red circle suggests five neighbors (when  $k = 5$ ) considering the least Euclidean distance from data point A, and the green circle does the same for data point B. Now, the average of the five neighbors inside the red circle is computed to assign the prediction of data point A, and a similar procedure is followed for data point B.

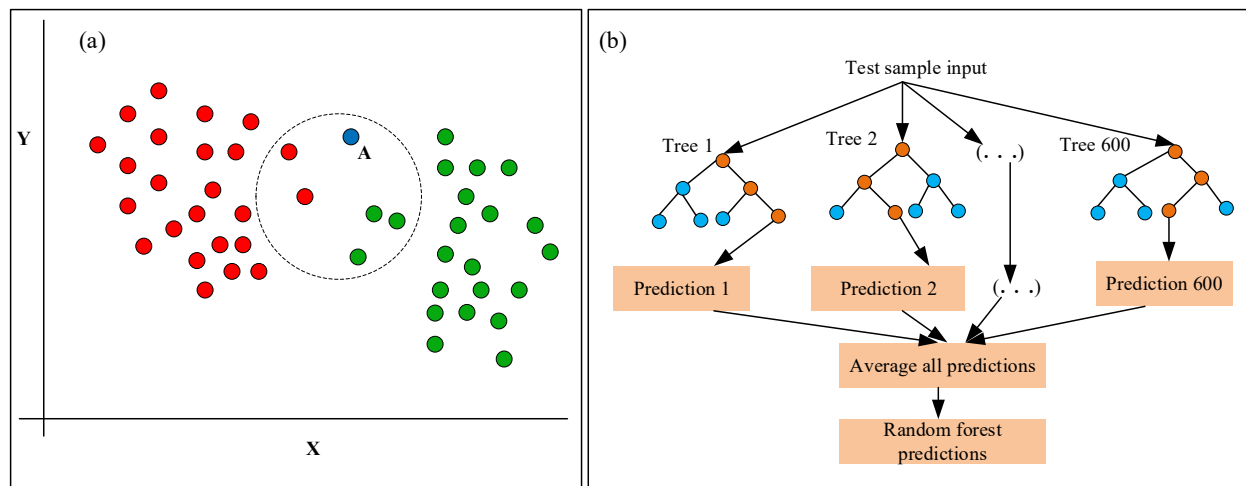


**Figure 4.** (a) KNN model architecture and (b) random forest architecture.

### 3.4. Random Forest Regressor

Random forest regressor is a powerful ensemble machine learning algorithm for classification and regression analysis. Primarily, bootstrap samples are generated according to the number of trees, with each tree being assigned a different bootstrap sample. This process ensures that each tree receives a different subset of data to be trained, eventually reducing the overfitting of the data. The decision to determine the optimal number of trees ( $n_{estimators}$ ) should be evaluated through a parametric study, preferably with GridSearchCV, to achieve the best learning outcome.

In a tree, the number of features will be the same as the original input. However, after that, each tree will create a root node that will evaluate all the features and decide only the best features and corresponding threshold values to split the data into two or more child decision nodes, aiming to minimize the variance for regression. Additional splits continue to be generated based on the selected features and threshold to further reduce the variance

of the training data. Finally, when the variance reaches its minimum, the splitting condition is met, and there, it forms leaf nodes, which are also called terminal nodes.

Now, when test data are provided, they reach the specific leaf node among all the leaf nodes created by each tree based on decision splits. The final prediction is made by averaging all the training data points of particular leaf nodes of the trees. It is also important to note that no interaction occurs among the trees, as illustrated in Figure 4b [40].

### 3.5. Application of Machine Learning to the Present Study

Datasets were collected from Ansys to train the machine learning models, such as multivariable linear regression, polynomial regression, random forest and KNN regressor algorithms. After that, features were selected in such a way that the feature scaling did not vary significantly. It was identified that during training, the volume of the stiffened panels caused a significant scaling problem, as the porosity, volume fraction, weight in kg and critical buckling load in kN were within small ranges of values, such as 0.1, 0.2, or 3, 5, 7 etc. On the other hand, volume was within the 100 to 2000 g/cm<sup>3</sup> scale range, which generated a scaling discrepancy. Therefore, volume was removed as a feature. Next, it was important to transform the categorical data to numeric values for training purposes. For the present case study, “Type of lattice structure” formed the categorical data, which were converted to numerical data using one-hot encoding, as shown in Figure 5.

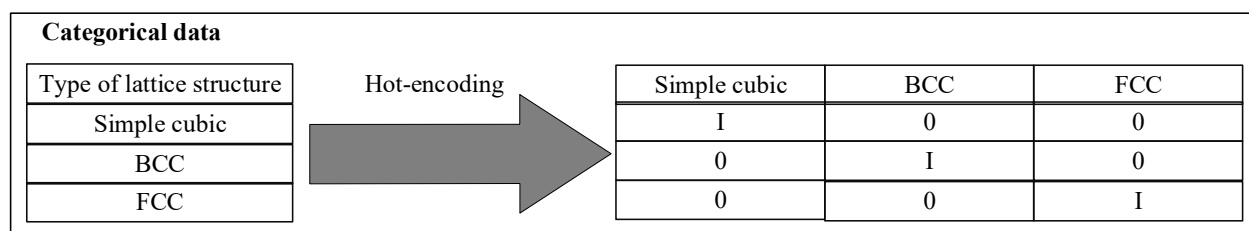


Figure 5. Hot encoding of categorical data.

The datasets were split into an 80–20% ratio for training and testing purposes. For polynomial regression,  $n$ —degree; for random forest,  $n$ —tree; and for KNN, the number of neighbors ( $K$ ) was optimized using the GridSearchCV algorithm to achieve the best results from the training.

After the training was completed, regression metrics such as mean squared error (MSE), root mean squared error (RMSE), mean absolute error (MAE) and  $R^2$  score were compared among the algorithms to find the best machine learning model for the present study. A process flow is depicted in Figure 6.

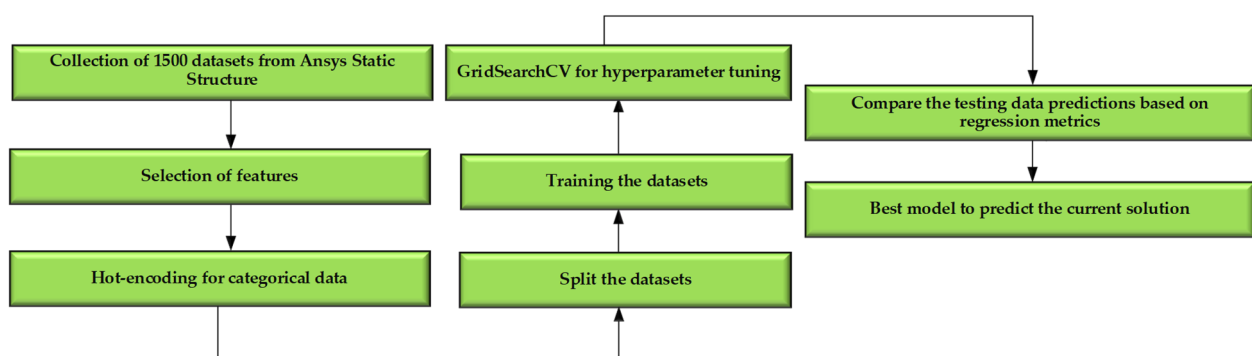


Figure 6. Machine learning workflow for the present study.



#### 4. Finite Element Validation

To gain confidence in the numerical outcomes, two different validations were conducted using the available literature. The first validation was based on the critical buckling load of aircraft-stiffened and sub-stiffened panels [33], while the second one was based on the critical buckling load of simple cubic lattice columns [22].

Considering the imperfections in the material, the complexity of the geometry of the stiffened and sub-stiffened panels, and the boundary conditions, the numerical prediction of the critical buckling load aligns well with the experimental values, as shown in Table 1. Moreover, the predicted buckling mode shape, illustrated in Figure 7 for both the stiffened and sub-stiffened panels, perfectly captures the experimental observations.

**Table 1.** Experimental and numerical buckling load of aircraft panels.

No.	Type of Panel	Experimental Buckling Load in KN [33]	Numerical Buckling Load in KN	Error in % $\left  \frac{Exp. - Numerical}{Exp.} \times 100\% \right $
1.	Stiffened Panel	74.5	72.337	2.9
2.	Sub-Stiffened Panel	140.2	148.9	6.2

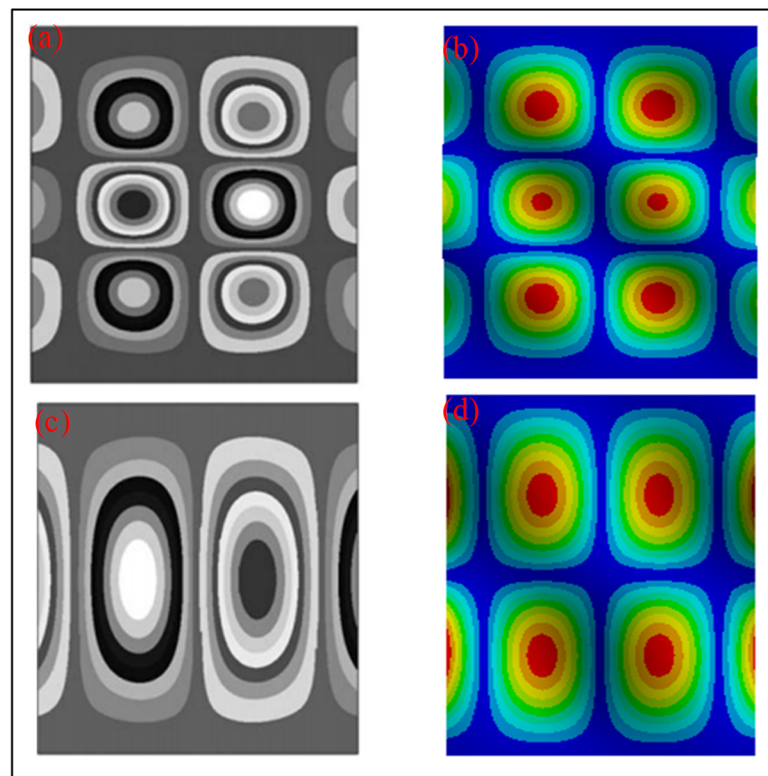


**Figure 7.** (a) Experimentally observed buckling mode of stiffened panel [33], (b) numerical buckling mode of stiffened panel, (c) experimentally observed buckling mode of stiffened panel [33], (d) numerical buckling mode of sub-stiffened panel.

For the simple cubic lattice column, numerical simulations can accurately predict the experimental buckling load, as shown in Table 2, where the error percentage falls within the 10% limit for most cases. This accuracy is notable, as the polymer columns are made using additive manufacturing, where slight changes in strut thickness are common, and deviations between the designed and printed models can significantly affect the critical buckling load of the column.

**Table 2.** Experimental and numerical buckling load of additively manufactured cellular columns.

Exp. No.	Sample Height, mm	Unit Cell Size, mm	h/wRatio	Experimental Buckling Load in N [22]	Numerical Buckling Load in N	Error in % $\left  \frac{Exp.-Numerical}{Exp.} \times 100\% \right $
1	201.2	2.5	10	2054	2245.8	9.3
2	201.2	4.74	10	3565	3105.4	12.9
3	201.2	8.72	10	4485	3807.6	15.1
4	161.2	2.5	8	3343	3578.4	7
5	161.2	4.74	8	3989	3760.8	5.7
6	161.2	8.72	8	4329	4162.9	3.8
7	121.2	2.5	6	3159	3370.5	6.6
8	121.2	4.74	6	4437	4797.9	8.1
9	121.2	8.72	6	5228	5051.6	3.3
10	81.2	2.5	4	4750	4913.1	3.4
11	81.2	4.74	4	5155	4988.8	3.2
12	81.2	8.72	4	5746	5793.5	0.8

## 5. Results and Discussions

At first, the critical buckling mode shape was examined for the lattice-stiffened panels, and it was observed that for all the cubic cells, the panels experienced a similar buckling mode, which was global and identical to that of a solid stiffened panel with the same geometric configurations, as illustrated in Figure 8.

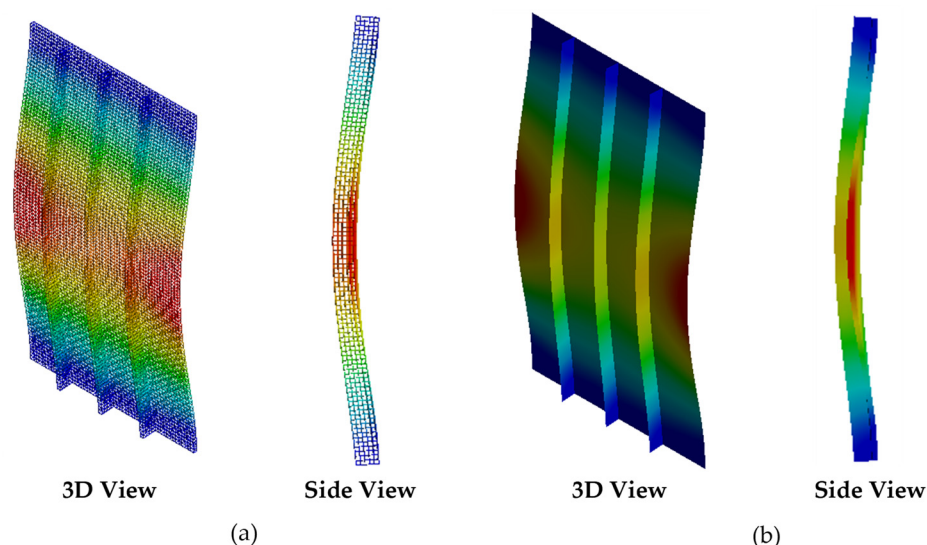


**Figure 8.** (a) Buckling mode shape of lattice-stiffened panel, (b) buckling mode shape of solid stiffened panel.

Next, the results were observed for the lattice-stiffened panels by increasing the strut diameter from 0.5 mm to 2 mm for all the different configuration of unit cells, as illustrated in Figure 9. It was observed that the load-carrying capacity of the panels increased exponentially, demonstrating a non-linear relationship between the strut diameter and the critical buckling load. As expected, with each increment in diameter, the critical buckling load of the FCC, BCC and simple cubic panels increased significantly. For the FCC panel, increasing the diameter from 0.5 mm to 2 mm resulted in an increase in the critical buckling load from 10.8 KN to 330.51 KN, which is an increase of 2938%. For other lattice

panels, namely for simple cubic and FCC panels, the percentage increases were 4800% and 2818%, respectively.

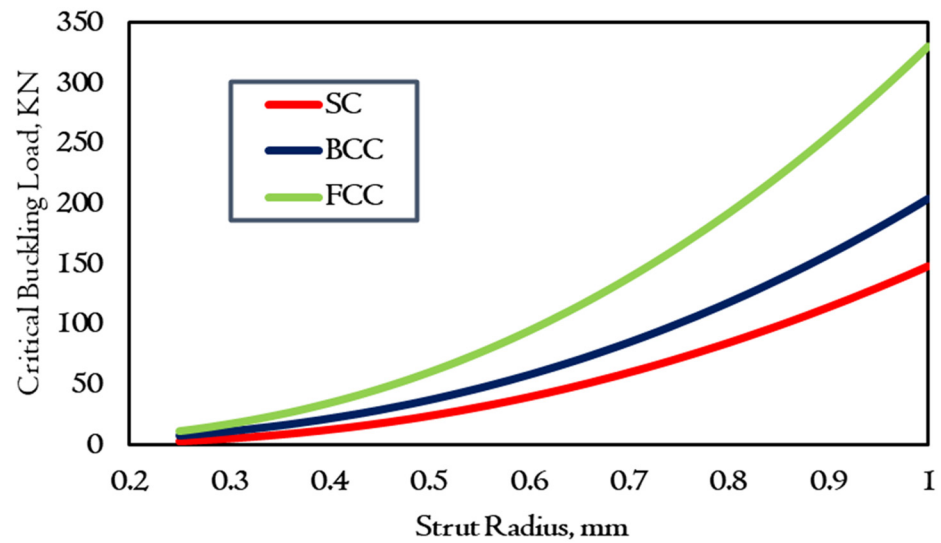


**Figure 9.** Critical buckling load against strut radius.

The reason behind the higher buckling load of FCC is that it had 24 struts, while BCC and simple cubic panels had 16 and 12 struts, respectively. However, these results do not provide the whole picture of the critical buckling load of these panels, as the diameter increase would result in a weight increase. Nevertheless, for lattice panels, relative density (or porosity) and fixed density (fixed porosity) are two crucial parameters to consider, which are discussed next.

Relative density is the ratio between the density of the lattice cell and the density of the corresponding solid material. For lattice structures, a lower density signifies a more lightweight design. On the other hand, porosity ( $n$ ), which is a measurement of the void space of a unit cell, indicates how much lighter the design is. The relationship between relative density and porosity is given as follows: porosity for a lattice structure =  $1 - \text{relative density}$ . Both the results for relative density and the porosity are illustrated in Figures 10 and 11. Considering the relative density and porosity of the lattice panel, it was found that the simple cubic lattice panel is better for resisting buckling when compared to BCC and FCC panels. For instance, when the relative density is 20%, or the weight of the panel is 20% of the solid lattice panel (Figure 10), and porosity is 80%, or the void space is 80% (Figure 11), the critical buckling load of the simple cubic panel is 25.46 KN, which is almost 50% higher than that of FCC and BCC panels. For 30% and 40% relative densities, the percentage of higher buckling value is 71% and 77%, respectively. It is also interesting to see how the FCC and BCC structures exhibit almost similar buckling results at up to 50% relative density. Further increasing the relative density suggests a higher critical buckling load for the FCC structure, which is almost 14% when the relative density of the panels is 60%, or it has 40% void space in terms of porosity. Next, the results are plotted for fixed relative density, as shown in Figure 12. Fixed relative density is the ratio between the density of the lattice and the solid material, where the solid block's density is considered fixed. To be more precise, if the diameter of the strut is increased, the volume of the lattice cell is increased accordingly. However, for a fixed relative volume, the ratio only considers that the solid volume will not change with the volume of the lattice.

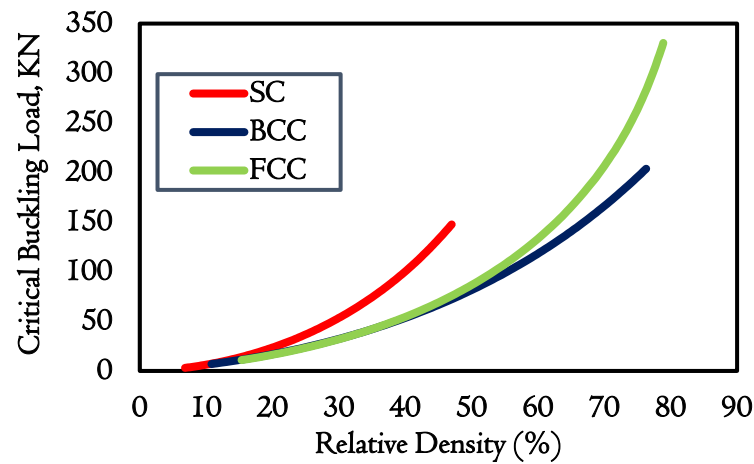


Figure 10. Critical buckling load against relative density.

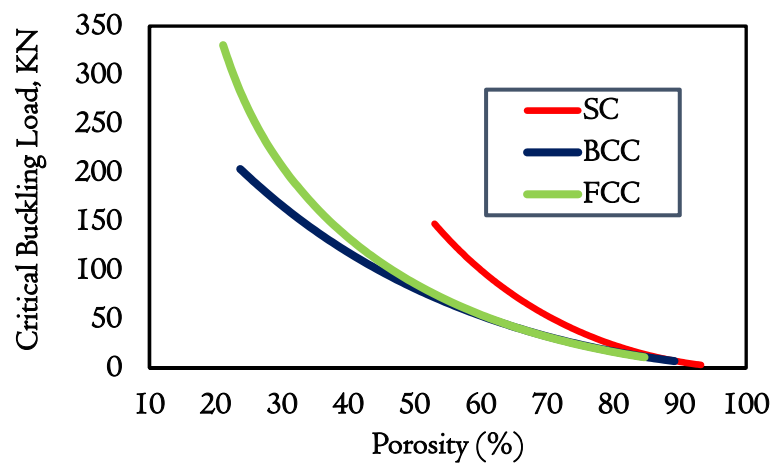


Figure 11. Critical buckling load against porosity.

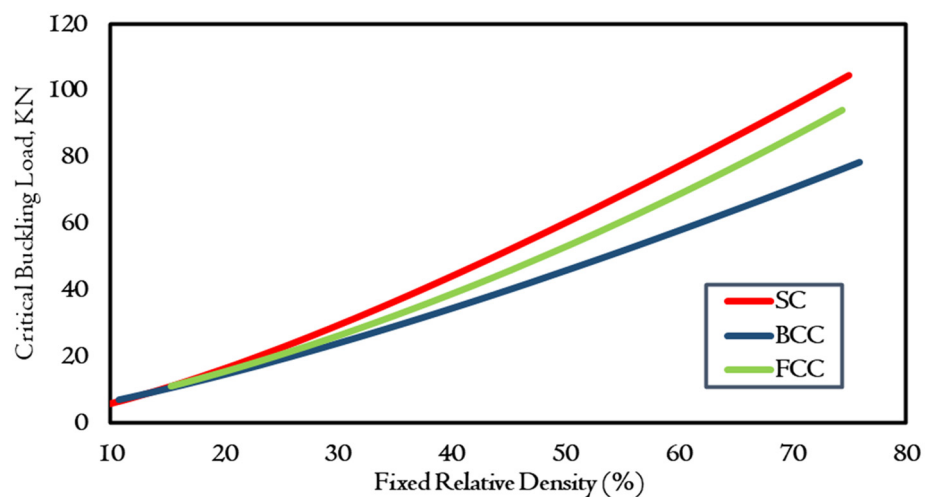


Figure 12. Critical buckling load against fixed relative density.

The numerical outcomes in Figure 12 suggest that increasing the fixed relative volume will increase the critical buckling load of the panel for all lattice configurations. However, for the simple cubic lattice structure, the critical buckling load is moderately higher than that of the FCC structure and significantly higher than that of the BCC panels. For a fixed relative density of 30%, the simple cubic panel shows about 25% and 13% higher buckling loads than BCC and FCC structures, respectively. However, for higher fixed

relative densities, the simple cubic panel exhibits approximately a 10% to 12% higher buckling load than the FCC panel up to a 70% relative density. Notably, for the case of BCC panels, this difference is much larger, and as the fixed relative density increases, the difference in critical buckling load between the panels increases drastically, reaching 28% for a fixed relative density of 50% and up to 30% when the value is 70%.

#### Machine Learning Results

In this section, results are discussed based on the ML algorithms, which are compared using four regression evaluation metrics, namely MAE, MSE, RMSE and  $R^2$  score. MAE is a straightforward error calculator that predicts the average error between the predicted and the actual data. Sometimes, it can omit large errors, as it gives the average error of the dataset. On the other hand, MSE calculates the average squared errors of the predicted and actual dataset. It can penalize large errors, making MSE values significant for precision. RMSE is the square root of MSE, which brings the error back to its original unit, making it more interpretable. Finally, the  $R^2$  score is useful for studying how well the predicted model captures the variance of the test data. The  $R^2$  score measures the proportion of the variance in the target variable that is explained by the model. Practically, a value of 1 suggests a perfect fit of the trained model, meaning it can explain all the variance, while a value of 0 suggests that the model has completely failed to capture the variance of the original data.

Looking at the MAE results, as illustrated in Figure 13, it is found that polynomial regression achieves the least MAE, with a value of 0.0077, outperforming all other models. On the other hand, KNN and random forest also provide acceptable MAE, 0.1786 and 0.7145, respectively, while multivariable regression exhibits the highest MAE of 9.3553. As expected, the value of MSE is significantly higher, at 172.4944 for multivariable regression, as shown in Figure 14. However, KNN performs quite well, with a value of 0.1792, while polynomial regression suggests a negligible value of MSE: to be exact, 0.0001. Next, RMSE results are shown in Figure 15: these suggest that both KNN and polynomial regression offer excellent values of 0.0105 and 0.4233, respectively, suggesting almost errorless predictions of the critical buckling load. Finally, the  $R^2$  score, as depicted in Figure 16, shows that KNN, polynomial regression and random forest can capture the variance of the original data with precisions of 0.9990, 0.9999 and 0.9942, respectively, which is excellent in terms of predictive performance and generalization to unseen data. In contrast, multivariable linear regression also performs reasonably well, with an  $R^2$  score of 0.96. In summary, it is found that all the models can explain the variance of the original data quite well, with polynomial regression consistently outperforming the others in terms of accuracy and error minimization.

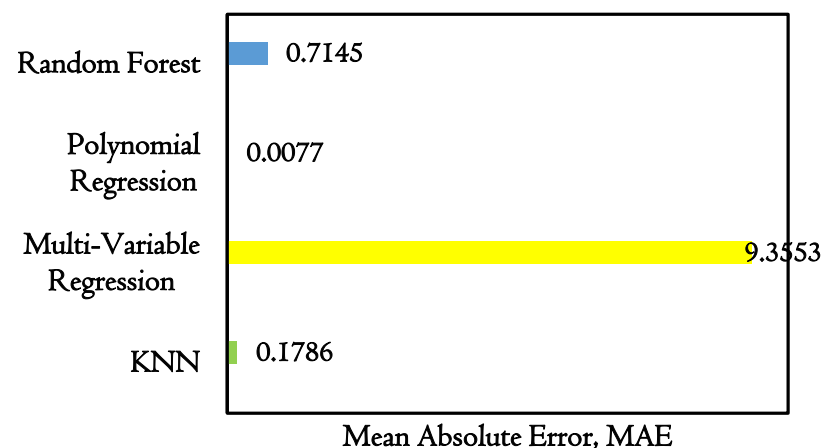


Figure 13. MAE results of the ML models.

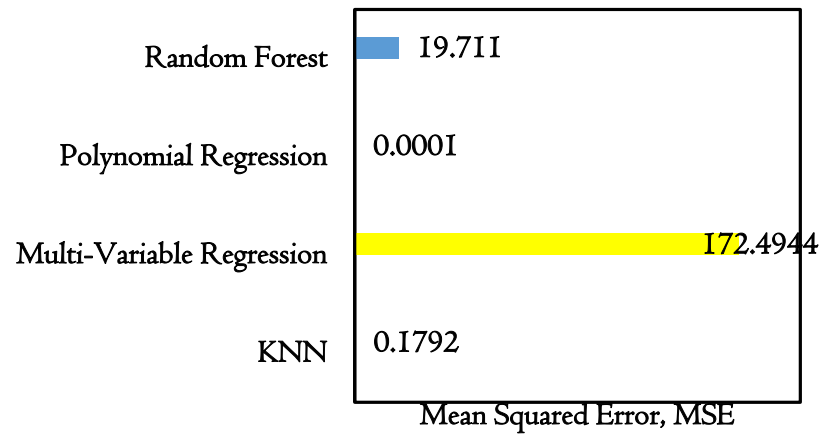


Figure 14. MSE results of the ML models.

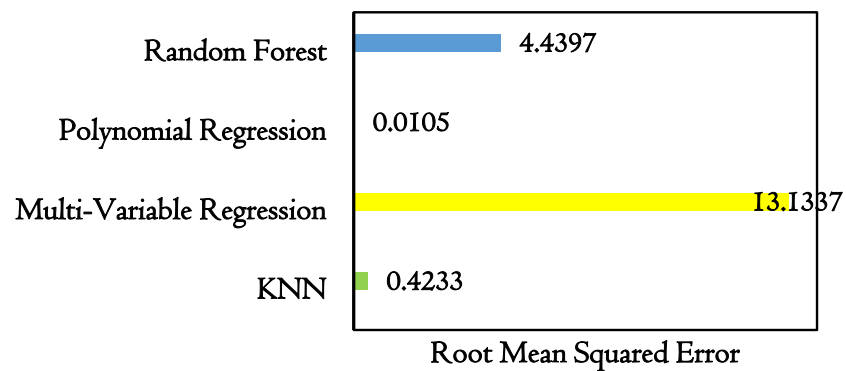


Figure 15. RMSE results of the ML models.

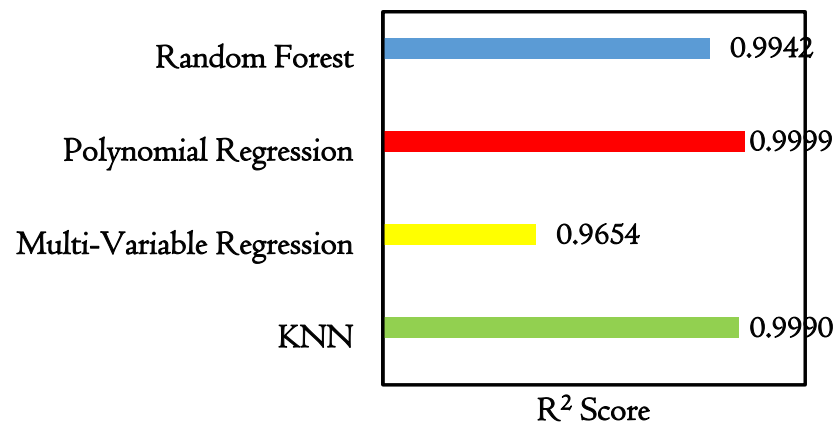
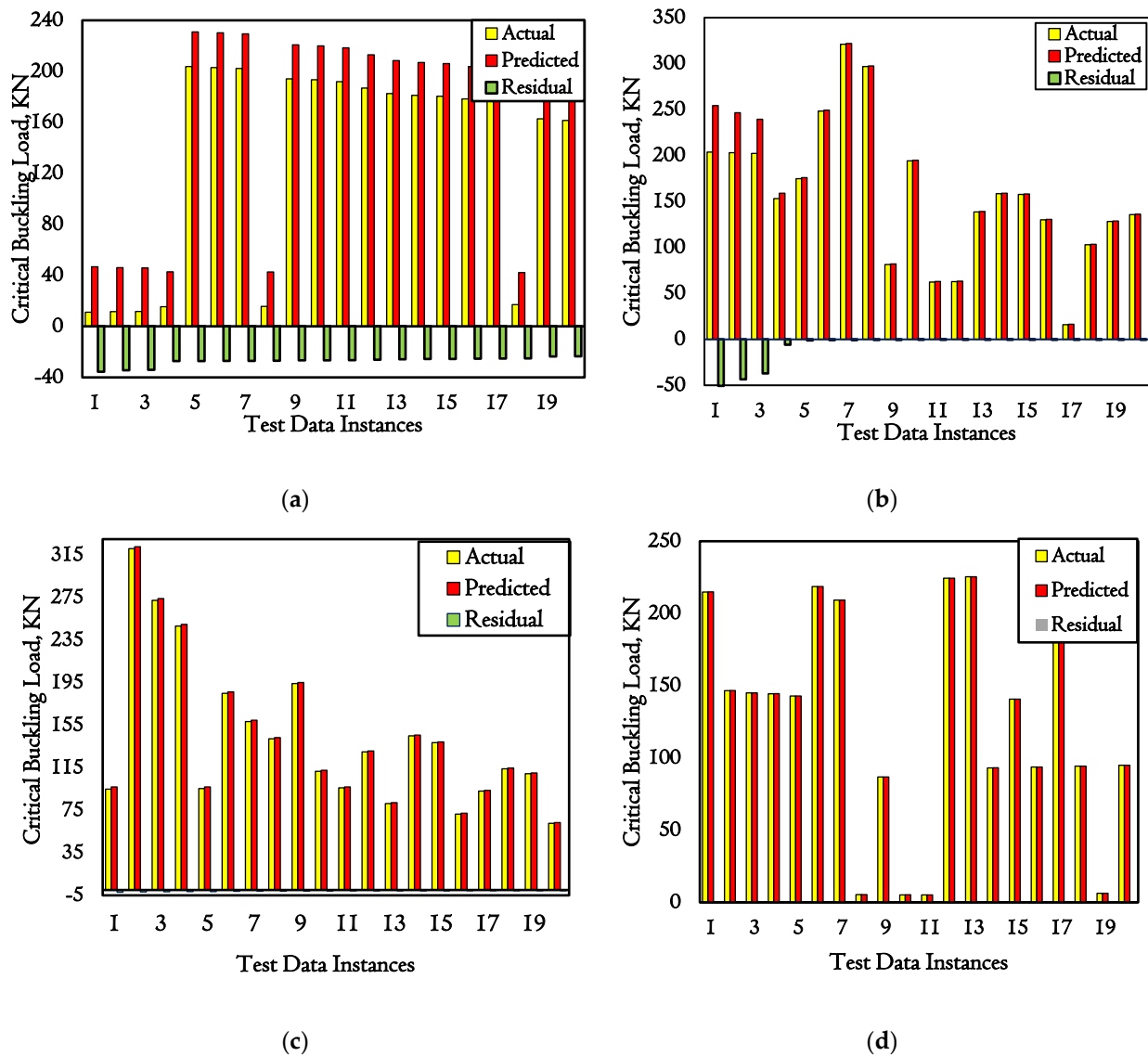


Figure 16. R<sup>2</sup> score of the ML models.

Next, results are plotted for the residuals of the tested data and the predicted data for 20 sample cases, sorted from largest to smallest residual values, as shown in Figure 17. Consistent with the evaluation metrics, the multivariable linear regression has residuals for all the predictions (Figure 17a); therefore, the value of MAE, MSE and RMSE is highest among all the models. In contrast, the random forest model has lower residuals compared to multivariable linear regression (Figure 17b). Interestingly, only for four instances does it exhibit a significant value of residuals, reaching 50. However, for the remaining instances, these residuals are quite low. These four instances mainly contribute to higher values of MSE, MAE and RMSE for the case of random forest regression.



**Figure 17.** (a) Residuals of multivariable linear regression; (b) residuals of random forest regressor; (c) residuals of KNN; (d) residuals of polynomial regression.

For KNN, as shown in Figure 17c, very small residuals are observed for only two instances, which are less than 5. However, besides these two, the rest of the cases suggest negligible residuals, leading to very low MSE, MAE and RMSE values, as discussed in the previous section. Finally, polynomial regression exhibits negligible residuals for all the data instances, as shown in Figure 17d, which results in the lowest MAE, MSE and RMSE values among all the models and a perfect  $R^2$  score.

## 6. Conclusions

The critical buckling load of aerospace-type stiffened panels made of three different cubic lattice cells, namely simple cubic, FCC and BCC structures, was investigated using Ansys software. Ti-4Al-6V was used as the base material, while the panel was fixed at its shorter edges and left free at its longer edges. Afterward, data samples generated from the numerical outcomes were collected to train four different ML algorithms to study their capability in predicting the critical buckling load of the lattice-stiffened panels. The main outcomes of the study are given as follows:

1. In the present investigation, a global buckling mode shape was observed for all the stiffened panels, similar to a solid counterpart with equivalent geometric parameters.
2. The critical buckling load increased with the increase in strut diameter, following a non-linear curve, and the load increase was exponential. As the FCC structure had the highest number of struts in a unit cell, it provided a higher critical buckling load among the investigated lattice cells. Changing the diameter from 0.5 mm to 2 mm resulted in an increase in the critical buckling load of about 2938% for the FCC panel, 4800% for the simple cubic panel and 2818% for the BCC panel.
3. Considering the relative density and the porosity of the panels, it was found that the simple cubic lattice cell had a better critical buckling capacity, which was 50% higher than both BCC and FCC structures at a relative density of 20%. With increased relative density, this gap further extended to 71% and 77% for relative densities of 30% and 40%, respectively.
4. Even when considering fixed relative density, the simple cubic lattice panel outperformed both FCC and BCC panels. It showed around 25% and 13% higher buckling loads than the BCC and FCC panels, respectively, at a 30% fixed relative density.
5. Among the compared ML models, polynomial regression provided the highest accuracy with the lowest MAE (0.007), MSE (0.0001), RMSE (0.0105) and a perfect  $R^2$  score of 0.9999. However, KNN also performed reasonably well and can provide excellent buckling load predictions.

While the current study highlights the potential of lattice structures for lightweight and efficient design, it is limited to linear buckling analysis, which assumes ideal conditions and does not account for material nonlinearities, imperfections, or post-buckling behavior. Future research should address these limitations by investigating the ultimate collapse load of lattice-stiffened panels, incorporating geometric imperfections and exploring nonlinear material properties. Additionally, the integration of advanced deep learning algorithms could further enhance the predictive accuracy of these complex panels. Such advancements would contribute to the broader application of lattice structures in aerospace and other high-performance industries, where the balance between lightweight design and structural safety is significant.

**Supplementary Materials:** The following supporting information can be downloaded at: <https://www.mdpi.com/article/10.3390/met15010081/s1>.

**Author Contributions:** Conceptualization, S.B.R.; methodology, S.B.R., S.S. and G.V.; software, S.B.R., M.M.R. and J.S.; validation, M.M.R. and J.S.; formal analysis, S.B.R., M.M.R. and J.S.; investigation, S.B.R., S.S. and G.V.; resources, S.B.R. and S.S.; data curation, S.B.R. and M.M.R.; writing—original draft preparation, S.B.R. and M.M.R.; writing—review and editing, J.S., S.S. and G.V.; visualization, S.B.R. and M.M.R.; supervision, S.B.R. and G.V.; project administration, S.S. and G.V.; funding acquisition, G.V. All authors have read and agreed to the published version of the manuscript.

**Funding:** This research received no external funding.

**Data Availability Statement:** The original contributions presented in this study are included in the article/Supplementary Material. Further inquiries can be directed to the corresponding authors.

**Acknowledgments:** Although this research was conducted without direct funding, the authors acknowledge the support of the University Grant Commission (UGC), Bangladesh, for funding the initial project (Research Code 3257103), which investigated the applicability of lattice structures in aircraft stiffened panels and laid the foundation for this work.

**Conflicts of Interest:** The authors declare no conflicts of interest.



## References

1. Hao, B.; Zhao, Y.; Zhu, Z. Study on the Mechanical Properties and Energy Absorption of Gyroid Sandwich Structures with Different Gradient Rules. *Arch. Appl. Mech.* **2024**, *94*, 3535–3553. [[CrossRef](#)]
2. Nagesha, B.K.; Dhinakaran, V.; Shree, M.V.; Kumar, K.P.M.; Chalawadi, D.; Sathish, T. Review on Characterization and Impacts of the Lattice Structure in Additive Manufacturing. *Mater. Today Proc.* **2020**, *21*, 916–919. [[CrossRef](#)]
3. Miao, X.; Hu, J.; Xu, Y.; Su, J.; Jing, Y. Review on Mechanical Properties of Metal Lattice Structures. *Compos. Struct.* **2024**, *342*, 118267. [[CrossRef](#)]
4. Hanks, B.; Berthel, J.; Frecker, M.; Simpson, T.W. Mechanical Properties of Additively Manufactured Metal Lattice Structures: Data Review and Design Interface. *Addit. Manuf.* **2020**, *35*, 101301. [[CrossRef](#)]
5. Harris, J.A.; Winter, R.E.; McShane, G.J. Impact Response of Additively Manufactured Metallic Hybrid Lattice Materials. *Int. J. Impact Eng.* **2017**, *104*, 177–191. [[CrossRef](#)]
6. Hasan, R.; Mines, R.; Shen, E.; Tsopanos, S.; Cantwell, W.; Brooks, W.; Sutcliffe, C. Comparison of the Drop Weight Impact Performance of Sandwich Panels with Aluminium Honeycomb and Titanium Alloy Micro Lattice Cores. *Appl. Mech. Mater.* **2010**, *24–25*, 413–418. [[CrossRef](#)]
7. Korner, M.E.H.; Lambán, M.P.; Albajez, J.A.; Santolaria, J.; Corrales, L.D.C.N.; Royo, J. Systematic Literature Review: Integration of Additive Manufacturing and Industry 4.0. *Metals* **2020**, *10*, 1061. [[CrossRef](#)]
8. Korkmaz, M.E.; Gupta, M.K.; Robak, G.; Moj, K.; Krolczyk, G.M.; Kuntoğlu, M. Development of Lattice Structure with Selective Laser Melting Process: A State of the Art on Properties, Future Trends and Challenges. *J. Manuf. Process.* **2022**, *81*, 1040–1063. [[CrossRef](#)]
9. Alomar, Z.; Concli, F. Compressive Behavior Assessment of a Newly Developed Circular Cell-Based Lattice Structure. *Mater. Des.* **2021**, *205*, 109716. [[CrossRef](#)]
10. Xiao, L.; Xu, X.; Feng, G.; Li, S.; Song, W.; Jiang, Z. Compressive Performance and Energy Absorption of Additively Manufactured Metallic Hybrid Lattice Structures. *Int. J. Mech. Sci.* **2022**, *219*, 107093. [[CrossRef](#)]
11. Wang, J.T.S.; Biggers, S.B. *Skin/Stiffener Interface Stresses in Composite Stiffened Panels*; NASA: Washington, DC, USA, 1984; Volume 3, pp. 1–29.
12. Ni, X.-Y.; Prusty, B.G.; Hellier, A.K. Buckling and Post-Buckling of Isotropic and Composite Stiffened Panels: A Review on Optimisation. *Int. J. Marit. Eng.* **2015**, *157*, A-9–A-29. [[CrossRef](#)]
13. Ni, X.-Y.; Prusty, B.G.; Hellier, A.K. Buckling and Post-Buckling of Isotropic and Composite Stiffened Panels: A Review on Analysis and Experiment (2000–2012). *Int. J. Marit. Eng.* **2016**, *158*, A-251–A-267. [[CrossRef](#)]
14. Chandra, D.; Satria, E.; Yusoff, N. Buckling Analysis of Curve Stiffened Fuselage Panel of Very Light Jet Aircraft. *IOP Conf. Ser. Mater. Sci. Eng.* **2021**, *1062*, 012049. [[CrossRef](#)]
15. Ge, J.; Huang, J.; Lei, Y.; O'Reilly, P.; Ahmed, M.; Zhang, C.; Yan, X.; Yin, S. Microstructural Features and Compressive Properties of SLM Ti6Al4V Lattice Structures. *Surf. Coat. Technol.* **2020**, *403*, 126419. [[CrossRef](#)]
16. Choy, S.Y.; Sun, C.N.; Leong, K.F.; Wei, J. Compressive Properties of Ti-6Al-4V Lattice Structures Fabricated by Selective Laser Melting: Design, Orientation and Density. *Addit. Manuf.* **2017**, *16*, 213–224. [[CrossRef](#)]
17. Qiu, C.; Yue, S.; Adkins, N.J.E.; Ward, M.; Hassanin, H.; Lee, P.D.; Withers, P.J.; Attallah, M.M. Influence of Processing Conditions on Strut Structure and Compressive Properties of Cellular Lattice Structures Fabricated by Selective Laser Melting. *Mater. Sci. Eng. A* **2015**, *628*, 188–197. [[CrossRef](#)]
18. Mazur, M.; Leary, M.; Sun, S.; Vcelka, M.; Shidid, D.; Brandt, M. Deformation and Failure Behaviour of Ti-6Al-4V Lattice Structures Manufactured by Selective Laser Melting (SLM). *Int. J. Adv. Manuf. Technol.* **2016**, *84*, 1391–1411. [[CrossRef](#)]
19. Bostan, B.; Kusbeci, M.; Cetin, M.; Kirca, M. Buckling Performance of Fuselage Panels Reinforced with Voronoi-Type Stiffeners. *Int. J. Mech. Sci.* **2023**, *240*, 107923. [[CrossRef](#)]
20. Lian, C.; Wang, P.; Zhang, K.; Yuan, K.; Zheng, J.; Yue, Z. Experimental and Numerical Research on the Calculation Methods for Buckling and Post-Buckling of Aircraft Tail Inclined Stiffened Panel under Compression Load. *Aerosp. Sci. Technol.* **2024**, *146*, 108930. [[CrossRef](#)]
21. Sarwoko, A.R.K.; Prabowo, A.R.; Ghanbari-Ghazijahani, T.; Do, Q.T.; Ridwan, R.; Hanif, M.I. Buckling of Thin-Walled Stiffened Panels in Transportation Structures: Benchmarking and Parametric Study. *Eng. Sci.* **2024**, *30*, 1137. [[CrossRef](#)]
22. Nazir, A.; Jeng, J.Y. Buckling Behavior of Additively Manufactured Cellular Columns: Experimental and Simulation Validation. *Mater. Des.* **2020**, *186*, 108349. [[CrossRef](#)]
23. Tang, H.; Li, L.; Hu, Y. Buckling Analysis of Two-Directionally Porous Beam. *Aerosp. Sci. Technol.* **2018**, *78*, 471–479. [[CrossRef](#)]
24. Mojtabaei, S.M.; Becque, J.; Hajirasouliha, I.; Khandan, R. Predicting the Buckling Behaviour of Thin-Walled Structural Elements Using Machine Learning Methods. *Thin-Walled Struct.* **2023**, *184*, 110518. [[CrossRef](#)]
25. Ly, H.B.; Le, T.T.; Le, L.M.; Tran, V.Q.; Le, V.M.; Vu, H.L.T.; Nguyen, Q.H.; Pham, B.T. Development of Hybrid Machine Learning Models for Predicting the Critical Buckling Load of I-Shaped Cellular Beams. *Appl. Sci.* **2019**, *9*, 5458. [[CrossRef](#)]

26. Kaveh, A.; Eslamlou, A.D.; Javadi, S.M.; Malek, N.G. Machine Learning Regression Approaches for Predicting the Ultimate Buckling Load of Variable-Stiffness Composite Cylinders. *Acta Mech.* **2021**, *232*, 921–931. [[CrossRef](#)]
27. Degtyarev, V.V.; Tsavdaridis, K.D. Buckling and Ultimate Load Prediction Models for Perforated Steel Beams Using Machine Learning Algorithms. *J. Build. Eng.* **2022**, *51*, 104316. [[CrossRef](#)]
28. Hu, S.; Wang, W.; Lu, Y. Explainable Machine Learning Models for Probabilistic Buckling Stress Prediction of Steel Shear Panel Dampers. *Eng. Struct.* **2023**, *288*, 116235. [[CrossRef](#)]
29. Tariq, A.; Uzun, B.; Deliktaş, B.; Yayli, M.Ö. A Machine Learning Approach for Buckling Analysis of a Bi-Directional FG Microbeam. *Microsyst. Technol.* **2024**. [[CrossRef](#)]
30. Kumar, R.; Kumar, A.; Kumar, D.R. Buckling Response of CNT Based Hybrid FG Plates Using Finite Element Method and Machine Learning Method. *Compos. Struct.* **2023**, *319*, 117204. [[CrossRef](#)]
31. Lee, H.G.; Sohn, J.M. Comparative Analysis of Buckling Pressure Prediction in Composite Cylindrical Shells Under External Loads Using Machine Learning. *J. Mar. Sci. Eng.* **2024**, *12*, 2301. [[CrossRef](#)]
32. Lee, Y.T.; Peters, M.; Welsch, G. Elastic Moduli and Tensile and Physical Properties of Heat-Treated and Quenched Powder Metallurgical Ti-6Al-4V Alloy. *Metall. Trans. A* **1991**, *22*, 709–714. [[CrossRef](#)]
33. Quinn, D.; Murphy, A.; McEwan, W.; Lemaitre, F. Stiffened Panel Stability Behaviour and Performance Gains with Plate Prismatic Sub-Stiffening. *Thin-Walled Struct.* **2009**, *47*, 1457–1468. [[CrossRef](#)]
34. Lee, H.; Wang, J.; Leblon, B. Using Linear Regression, Random Forests, and Support Vector Machine with Unmanned Aerial Vehicle Multispectral Images to Predict Canopy Nitrogen Weight in Corn. *Remote Sens.* **2020**, *12*, 2071. [[CrossRef](#)]
35. Timothy, O. Hodson Root-Mean-Square Error (RMSE) or Mean Absolute Error (MAE): When to Use Them or Not. *Geosci. Model Dev.* **2022**, *15*, 5481–5487. [[CrossRef](#)]
36. Benjaminson, E. Linear Regression and Gradient Descent. 2019. Available online: <https://sassafra13.github.io/LinReg/> (accessed on 17 December 2014).
37. Sharma, N. Multiple Linear Regression: Beyond Simple Linear Regression. 2023. Available online: <https://medium.com/@nitin.data1997/multiple-linear-regression-beyond-simple-linear-regression-b533cabff376> (accessed on 17 December 2024).
38. Ostertagová, E. Modelling Using Polynomial Regression. *Procedia Eng.* **2012**, *48*, 500–506. [[CrossRef](#)]
39. Feng, C.; Zhao, B.; Zhou, X.; Ding, X.; Shan, Z. An Enhanced Quantum K-Nearest Neighbor Classification Algorithm Based on Polar Distance. *Entropy* **2023**, *25*, 127. [[CrossRef](#)]
40. Chaya. Random Forest Regression. 2020. Available online: <https://levelup.gitconnected.com/random-forest-regression-209c0f354c84> (accessed on 17 December 2024).

**Disclaimer/Publisher’s Note:** The statements, opinions and data contained in all publications are solely those of the individual author(s) and contributor(s) and not of MDPI and/or the editor(s). MDPI and/or the editor(s) disclaim responsibility for any injury to people or property resulting from any ideas, methods, instructions or products referred to in the content.